ULTRASONIC NONDESTRUCTIVE EVALUATION USING NON-CONTACT AIR-COUPLED LAMB WAVES

by

Wenfeng Xiao

Bachelor of Science
Nanchang Hangkong University, 2012

Master of Engineering
Nanchang Hangkong University, 2015

Submitted in Partial Fulfillment of the Requirements

For the Degree of Doctor of Philosophy in

Mechanical Engineering

College of Engineering and Computing

University of South Carolina

2020

Accepted by:

Lingyu Yu, Major Professor

Victor Giurgiutiu, Committee Member

Yuh-Jin Chao, Committee Member

Bin Zhang, Committee Member

Cheryl L. Addy, Vice Provost and Dean of the Graduate School

CHAPTER 11

COMPOSITE MANUFACTURING QUALITY INSPECTION

Composites have been extensively used in aerospace engineering, renewable energies, and automotive industries due to the advantages of their lightweight, high strength, and engineering design flexibility. However, manufacturing defects, such as weak bonds and wrinkles may occur during manufacturing and will affect the performance of the structure and even lead to structural failure if not found timely. This chapter presents the inspection of certain selected manufacturing defects, including the adhesive bond quality evaluation and wrinkles in laminated composite structure using the noncontact ACT-SLDV Lamb wave method.

11.2 COMPOSITE WRINKLE INSPECTION

Today, laminated composites have been widely adopted in aerospace industries. Typically, a laminated composite consists of several layers of plies laminated together. During the manufacture of a thick composite by compression molding, a common problem is that plies may wrinkle, resulting in wrinkle defect in the composite [223]. This wrinkle defect in a laminated composite is a major problem because of its potential to compromise the mechanical properties of an intended design. In particular, a laminated composite with ply wrinkling is more susceptible to tensile and bending forces, making it impractical for the composite to perform its intended function, resulting in a lesser quality product. Therefore, the nondestructive evaluation of the wrinkle defects is critical to ensure the integrity of the composite structures and their safe operation as well.

We have performed wrinkle inspection using the noncontact ACT-SLDV method on certain wrinkle specimen. The wrinkle specimen is shown in Figure 11.12. The measured dimension of the sample plate is 306 × 205 × 3.74 (unit: mm). Significant wrinkles are observed from both surfaces as shown in Figure 11.12 (pointed by arrows). The areas with more visible wrinkles are marked as wrinkle region while that with less visible or likely no wrinkles as reference region. Please note no other information about the specimen is available to the inspectors. The predefined Cartesian coordinate is illustrated in Figure 11.12 and the detailed side views of the wrinkle damage and its location are presented in Figure 11.12c. It is noted that the wrinkle damage is visible in the range of x = 60 mm to x = 125 mm. In the reference region, a weak wrinkle defect is seen in the range of x = 190 mm to x = 220 mm, but the wrinkle is much less than the wrinkle region.

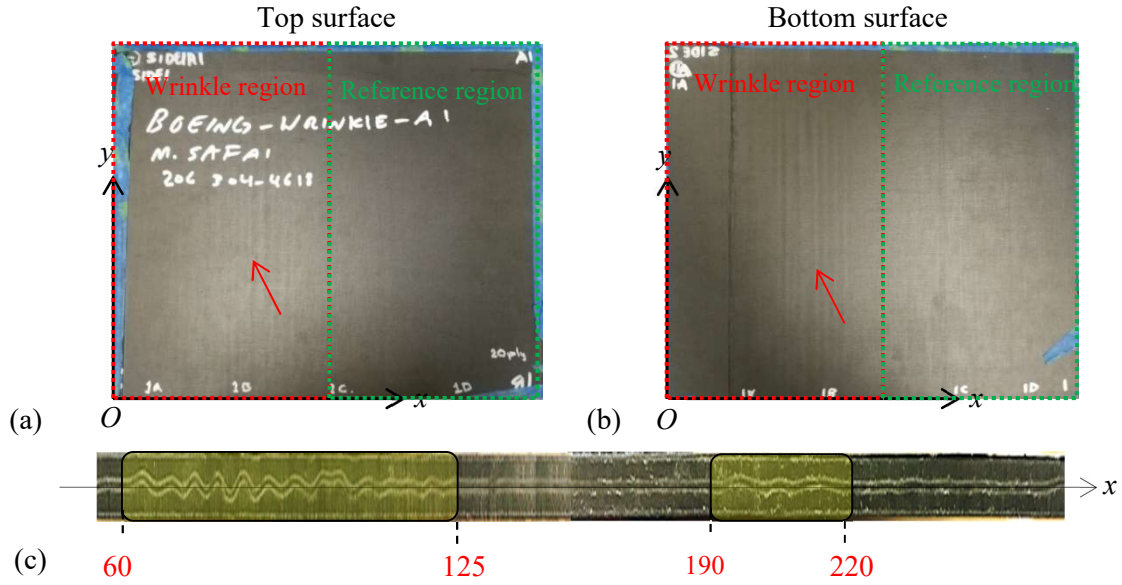
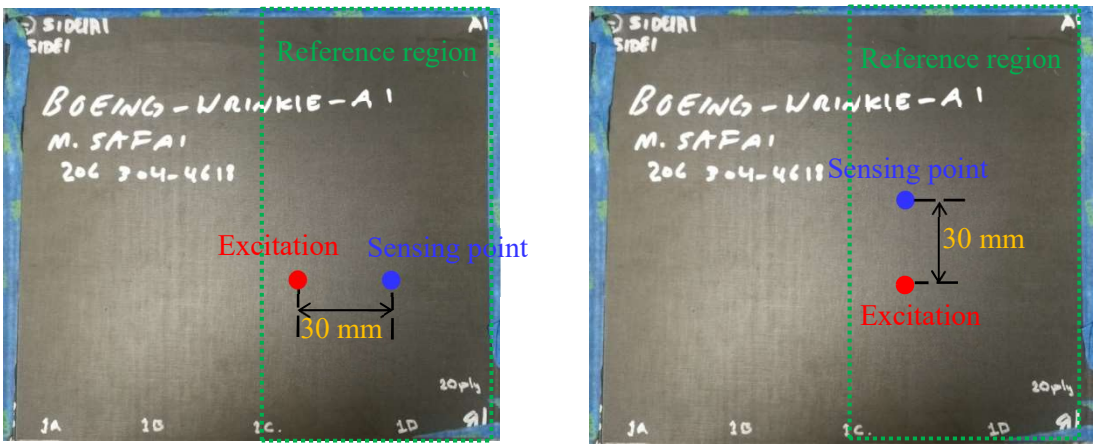


Figure 11.12: The composite specimen with wrinkle defects (Courtesy of NASA Langley Research Center and Boeing)

11.2.1 THE OPTIMAL INCIDENT ANGLES TUNING FOR ACT LAMB WAVES

To use the ACT for optimal Lamb wave signal excitation in the specimen, the incident angle θ tuning is first conducted in the reference region where the wrinkle is much less visible or likely none. The incident angle of the x-axis direction is conducted using the same experimental setup in Figure 11.2 with the ACT excitation and SLDV sensing location on the winkle sample as illustrated in Figure 11.13a. The Lamb wave signals are collected at 30 mm away from the excitation source at various incident angles at 10˚, 11˚, 13˚, 15˚, 17˚,19˚, and 20˚. Some representative signals are given in Figure 11.14 for illustration. It is noted that there is only one dominant wave package in the Lamb wave signal. The signal strength changes as the θ changes. The optimal angle is determined at which generates the maximum signal strength, where the signal strength is evaluated by the peak-to-peak value of the wave package (Figure 11.14b).



(a) (b)

Figure 11.13: The excitation and sensing location on the wrinkle sample for optimal incident angle tuning of (a) x-axis direction, (b) y-axis direction (Courtesy of NASA Langley Research Center and Boeing)

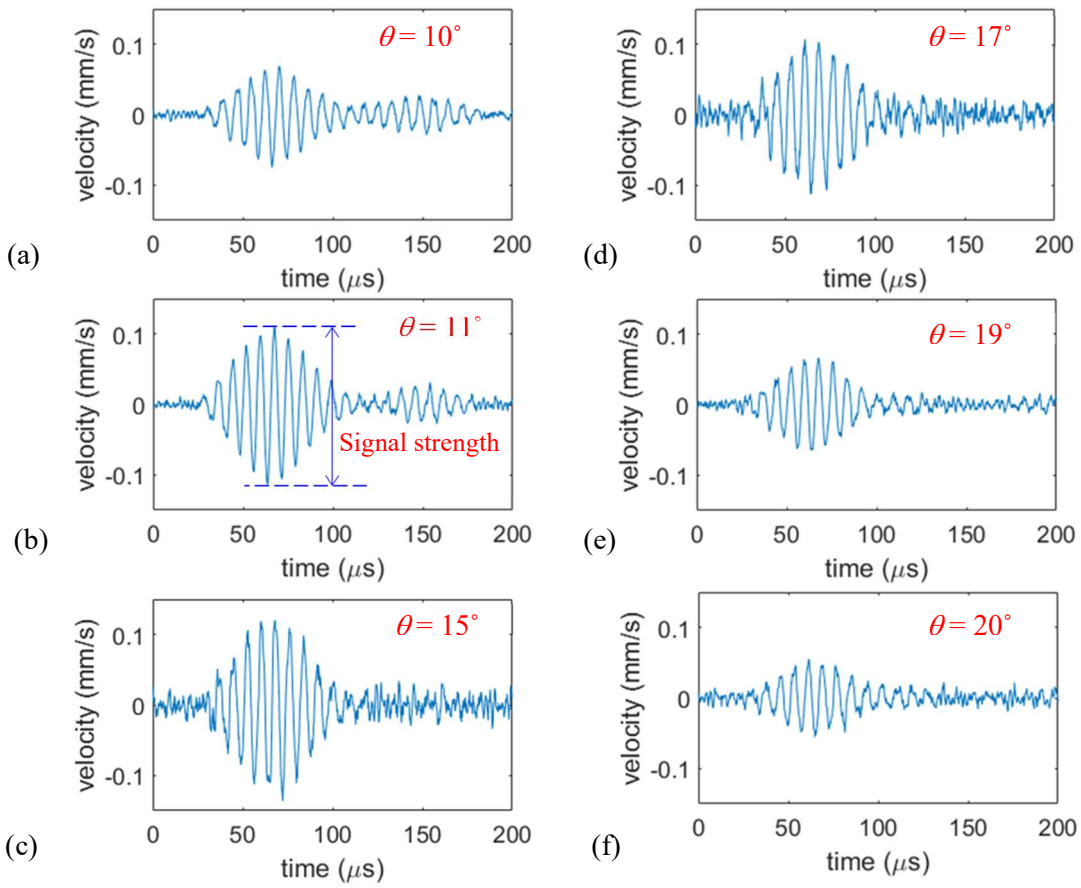


Figure 11.14: The optimal incident angle tuning along the *x*-axis direction. Results of (a) 10˚, (b) 11˚, (c) 15˚, (d) 17˚, (e) 19˚, and (f) 20˚

The signal quality at different incident angles is plotted in Figure 11.15. It is seen that as θ increases from 10˚ to 15˚, the signal strength increases and reaches its peak at 15˚. After θ increases from 15˚ to 20˚, the signal strength starts decreasing. Thus, it determined that the optimal Lamb wave incident angle along the *x*-axis direction is set at 15˚.

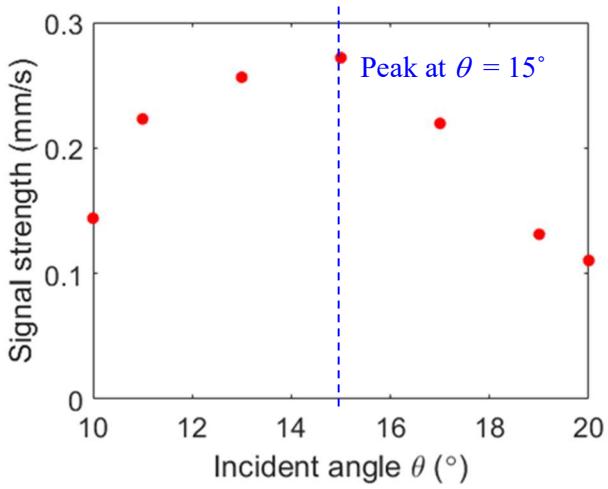


Figure 11.15: The optimal incident angle tuning result of *y*-axis direction

Similarly, the incident angle tuning for the *y*-axis direction orientated inspection is performed. Figure 11.16 presents the signals collected with the incident angles of 10˚, 11˚, 15˚, 17˚, 19˚, and 20˚, and the plot of signal quality at different incident angles is presented in Figure 11.17. It is seen that as θ increases from 10˚ to 15˚, the signal strength increases. The signal strength reaches its peak at 15˚, then as the θ increases from 15˚ to 20˚, the signal strength decreases. Therefore, the optimal Lamb wave incident angle along the *y*-axis direction is also determined at 15˚.

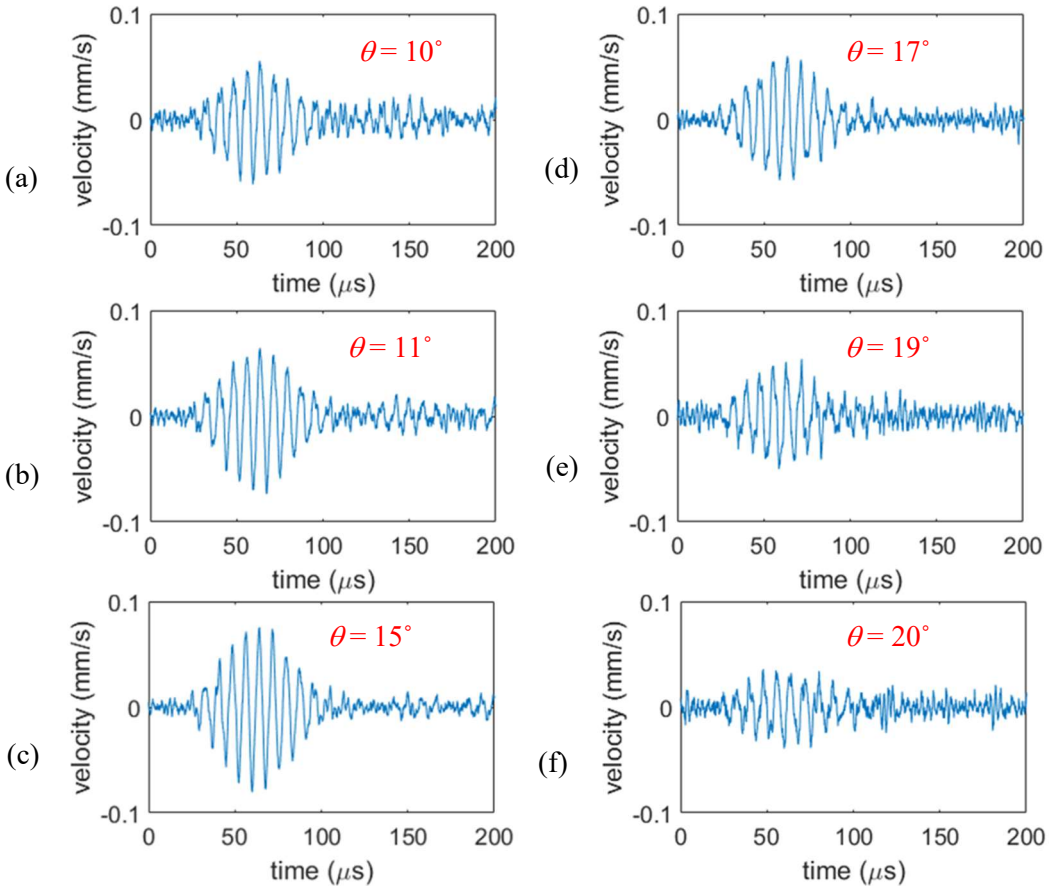


Figure 11.16: The optimal incident angle tuning along the *y*-axis direction. Results of (a) 10˚, (b) 11˚, (c) 15˚, (d) 17˚, (e) 19˚, and (f) 20˚

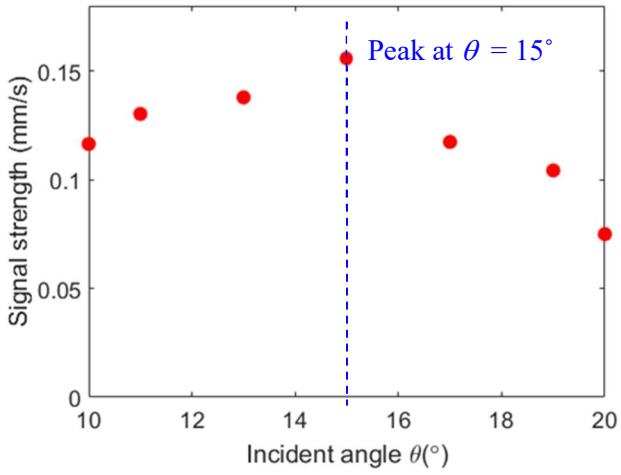


Figure 11.17: The optimal incident angle tuning result of *y*-axis direction

11.2.2 WRINKLE INSPECTION ALONG THE *X*-AXIS DIRECTION

With the incident angles being configured, the ACT-SLDV system is set up and first performed a quick 1D inspection by linescan along the *x*-axis direction. Both linescans in the wrinkle region and reference region are conducted for comparison purposes. Three linescans (W1, W2, and W3) in the wrinkle region and three linescans (R1, R2, and R3) in the reference region are performed. The setup of all the linescans is illustrated in Figure 11.18a.

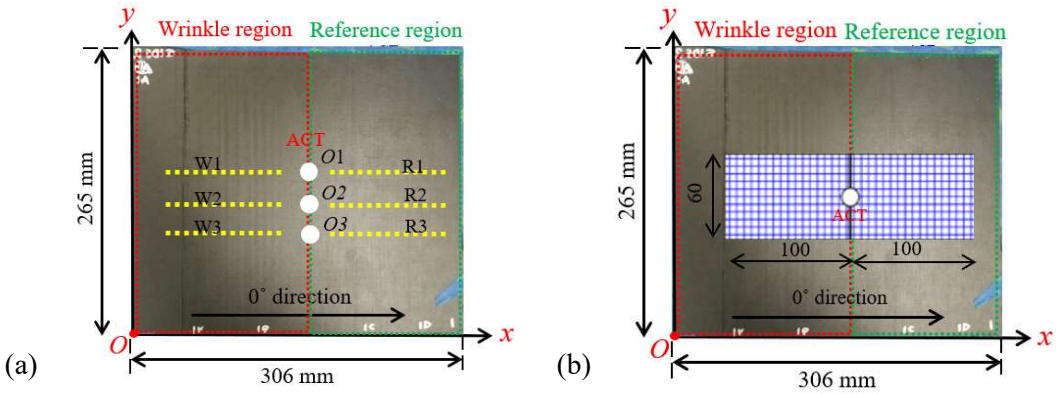


Figure 11.18: Experimental setup for *x*-axis direction (a) line inspection, and (b) area inspection (Courtesy of NASA Langley Research Center and Boeing)

The1D wavefields of linescan R1 and W1 are presented in Figure 11.19a and b, respectively. Little interactions in the R1 wavefield, but significant interactions with the contained wrinkles are observed in the W1 wavefield. The time-space wavefields are then transferred to the frequency-wavenumber domain by the 2DFT method outline in earlier chapters. The calculated frequency-wavenumber spectra of the R1 and W1 are presented in Figure 11.19c and d, respectively. Barely negative wavenumbers which related to the reflected waves are observed in the R1 spectrum, while negative wavenumbers in the W1 spectrum are noted which confirms that reflections are generated in the wrinkle region, indicating that the wrinkle signature is successfully captured through the linescan.

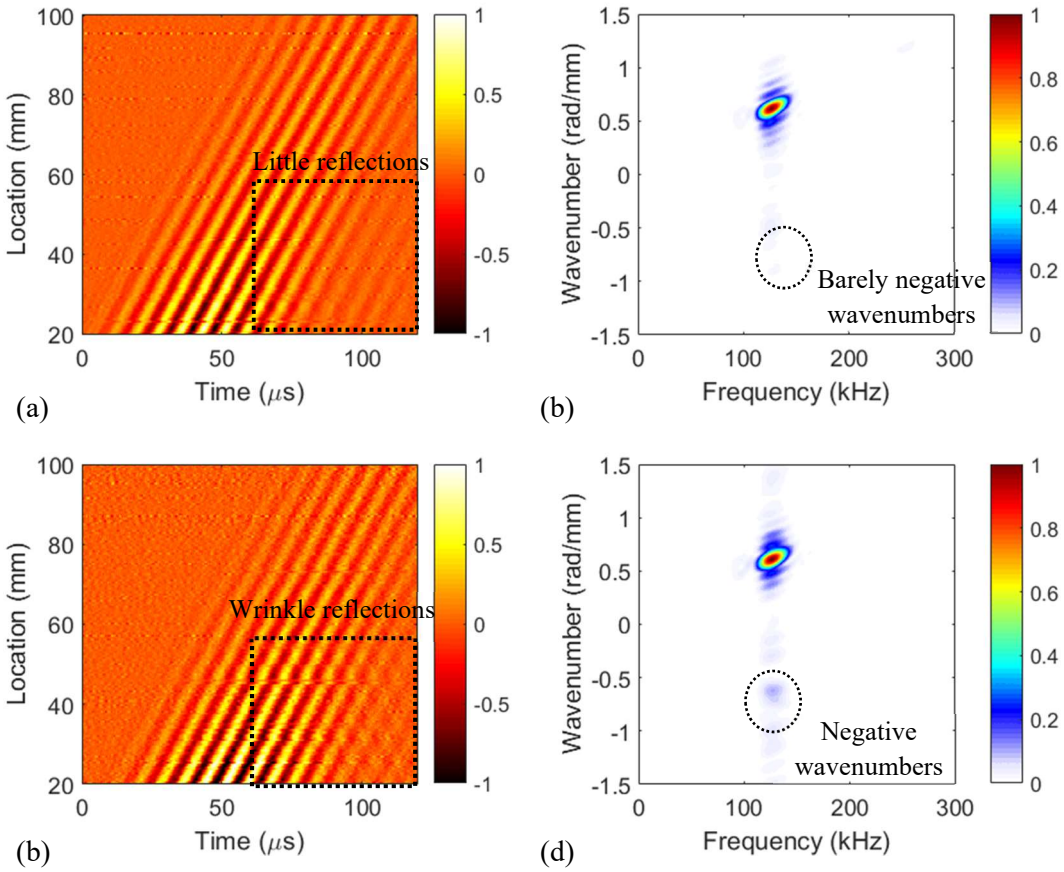


Figure 11.19 : 1D time-space wavefields of: (a) R1 and (b) W1, and (c) & (d) are their frequency-wavenumber spectrua, respectively

The 1D wavefields of R2 and W2 are shown in Figure 11.20a and b, respectively. Similarly, little reflections are noted in the R2 wavefield, but significant reflections are seen in the W2 wavefield. Their frequency wavenumber spectrum of the R1 and W2 wavefields are obtained by the 2DFT method as given in Figure 11.20c and d, respectively. The results show that barely negative wavenumbers which are related to the reflections are observed in the R2 spectrum while significant negative wavenumbers represent the reflections are seen in the W2 spectrum. The comparison of the R2 and W2 linescan result demonstrates that reflection signatures of the wrinkle are successfully captured and identified, resulting in the wrinkle is successfully detected.

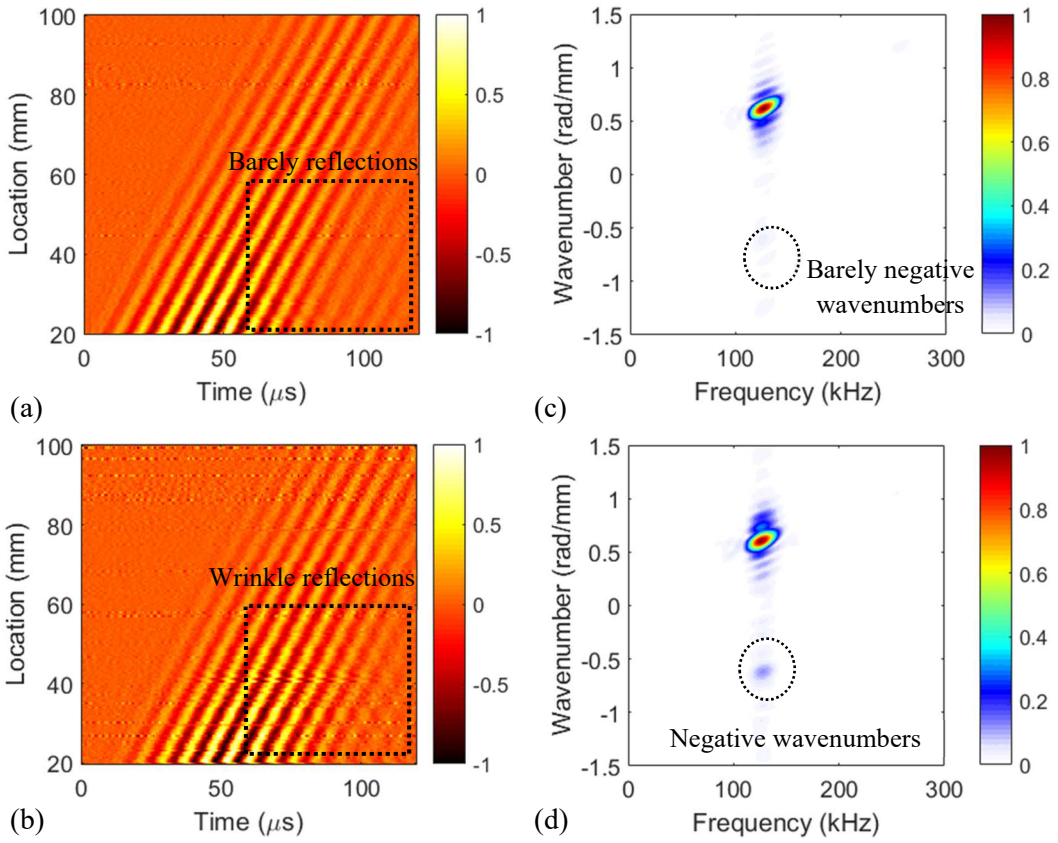


Figure 11.20 : 1D time-space wavefields of: (a) R2 and (b) W2, and (c) & (d) are their frequency-wavenumber spectrua, respectively

The collected 1D wavefields of R3 and W3 are given in Figure 11.21a and b, respectively. Weak reflections are noted in the R3 wavefield, which shows that subtle wrinkle is existing in the reference region. In the W3 wavefield, much stronger wrinkle reflections are noted as compared to the reference region. Their frequency wavenumber spectra are given in Figure 11.21c and d. Very weak reflections with negative numbers are noted in the R3 spectrum and the negative wavenumbers are also seen in the wrinkle region R3, which is consistent with the wavefield inspection. The inspection shows that wrinkle is detected in the wrinkle region, other than that, subtle reflections are also observed in the reference region, indicating that much fewer wrinkle defects are also existing in the reference region.

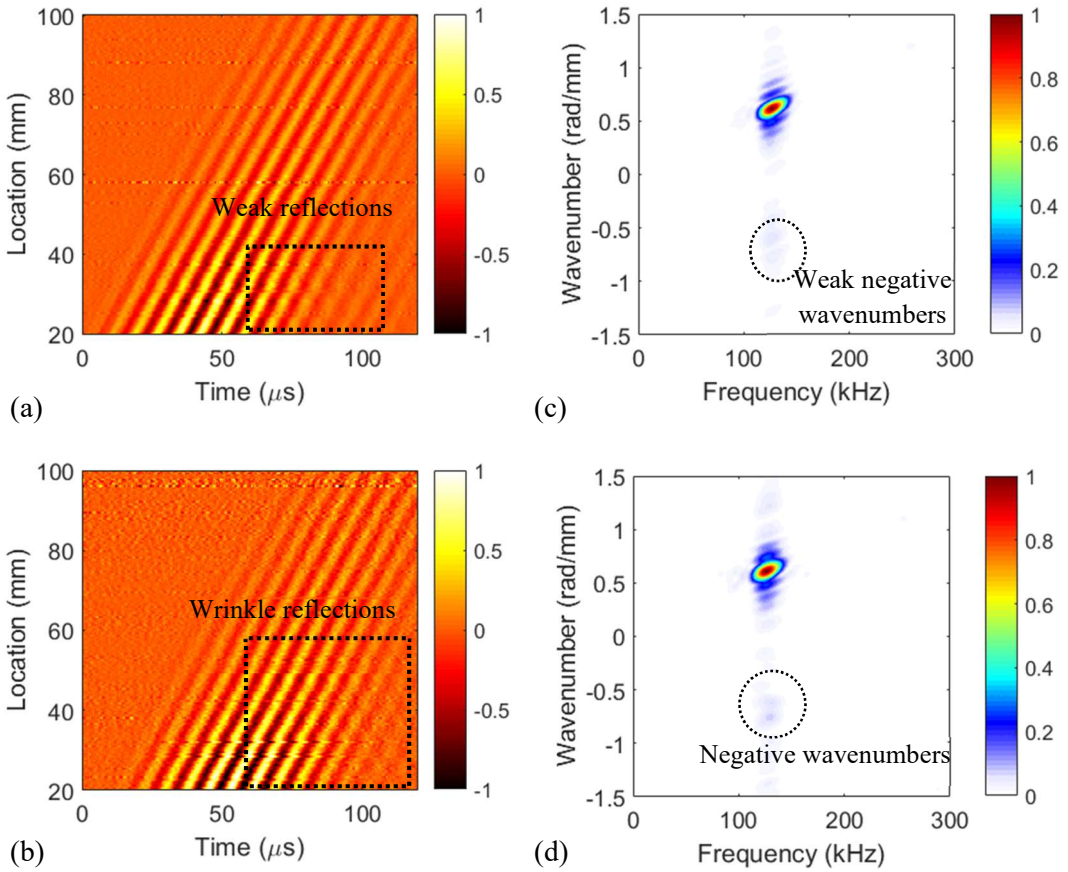


Figure 11.21 : 1D time-space wavefields of: (a) R3 and (b) W3, and (c) & (d) are their frequency-wavenumber spectrua, respectively

In the frequency wavenumber spectra, the negative wavenumbers which represent the reflected Lamb wave propagating back to the source are seen. However, the wavenumber distribution information along the propagating space is missing. Therefore, the short-space Fourier transform (STFT) algorithm is then used to get the wavenumber distribution along the propagation path. The wavenumber distribution along the propagation path from 20 to 100 mm at 120 kHz is presented in Figure 11.22a, b, and c for W1, W2, and W3 respectively. In the wavenumber-space spectrum, the positive wavenumber represents the incident waves that propagate forward, and negative wavenumbers represent the reflected waves that propagate back to the source.

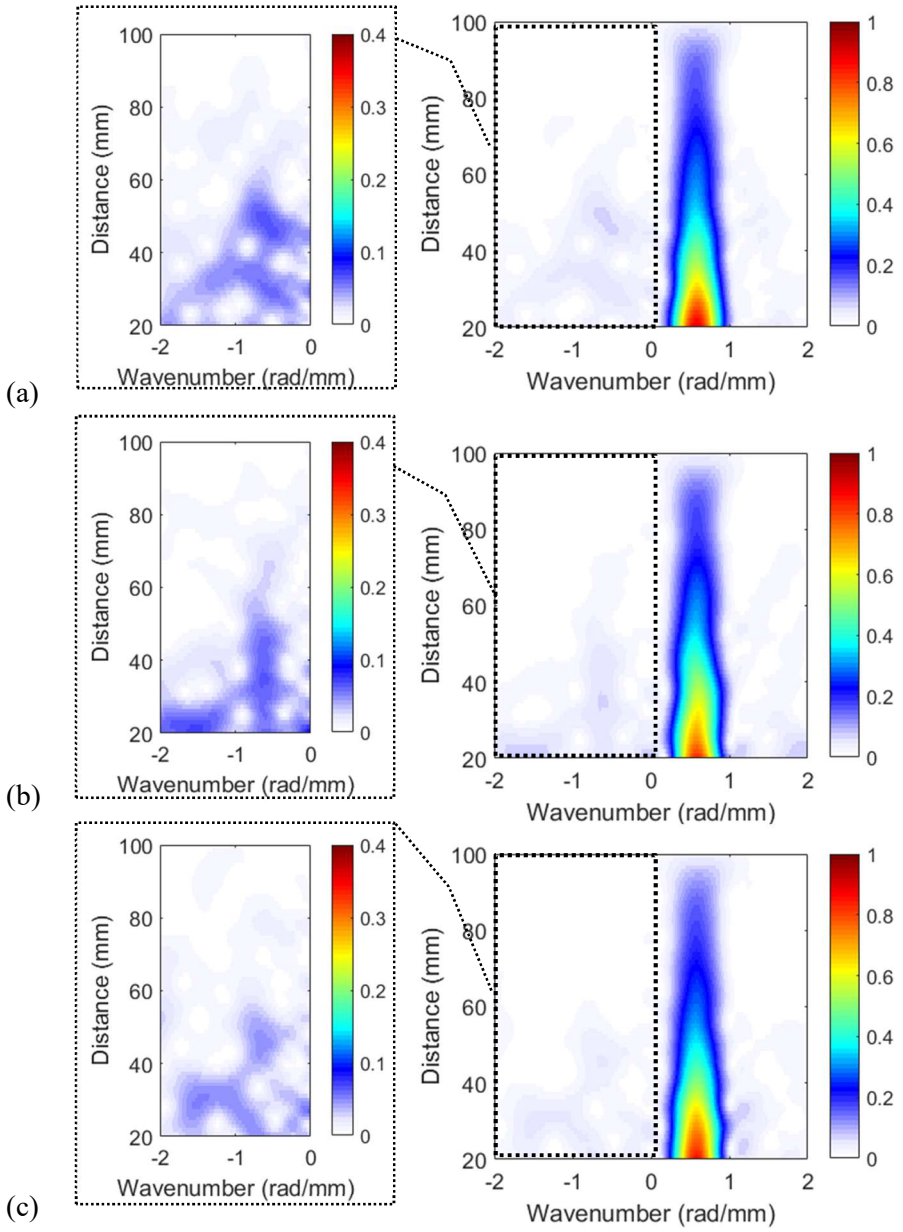


Figure 11.22: Wavenumber-space spectrum (a) W1, (b) W2, and (c) W3

In Figure 11.22, the strongest positive wavenumbers all are noted firstly at 20 mm which is the nearest distance to the source, then as the wave propagating forward, the wavenumber intensity decreased gradually due to the wave decaying in the structure. At about 60 mm location, the negative wavenumbers are introduced in the spectra, indicating that the reflections are generated at the wrinkle. The negative wavenumbers distribute from

60 mm to 20 mm, indicating that reflections propagating from 60 mm to 20 mm. The wavenumber space spectra of W1, W2, and W3 demonstrate the wavenumber signatures distribution in the wrinkle region, and the wrinkle is successfully detected through the linescan inspection.

2D area inspection by ACT was also further conducted to obtain more information and to observe the wave propagation more clearly. The area scan in both the reference region and wrinkle region is performed with the setup showing in Figure 11.18b. The snapshot of the wavefield at 25 μs, 60 μs, and 70 μs are given in Figure 11.23a, b, and c for wrinkle region, and Figure 11.23d, e, and f for reference region.

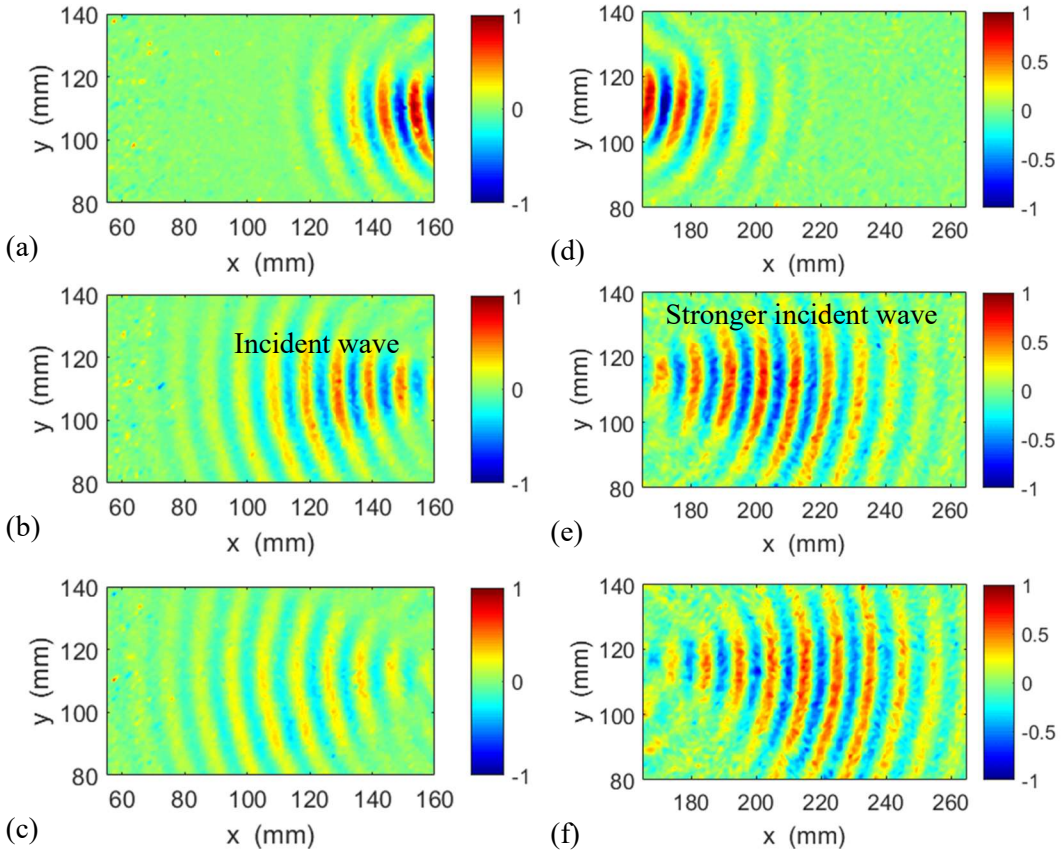


Figure 11.23: Wavefields of wrinkle region of (a) 25 μs, (b) 60 μs,and (c) 70 us; wavefields of reference region of (d) 25 μs, (e) 60 μs,and (f) 70 us with ACT actuaiton at x = 160 mm

The incident wave signatures propagating in the plate can be observed for both reference region and wrinkle region. No other significant wave interaction can be seen. But comparing the wave strength, it is seen that for the wrinkle region, the signal strength is weaker as compared to the reference regio and this may due to the wrinkle diffused the wave propagating in the plate in the wrinkle region.

Next, the energy map is generated to analyze the energy distribution map for inspection. The generated images are plotted in Figure 11.24a, b for the wrinkle region. In Figure 11.24a, the wrinkle in the range of 90 to 120 mm is successfully imagined and observed, demonstrating the wrinkle is inspected.

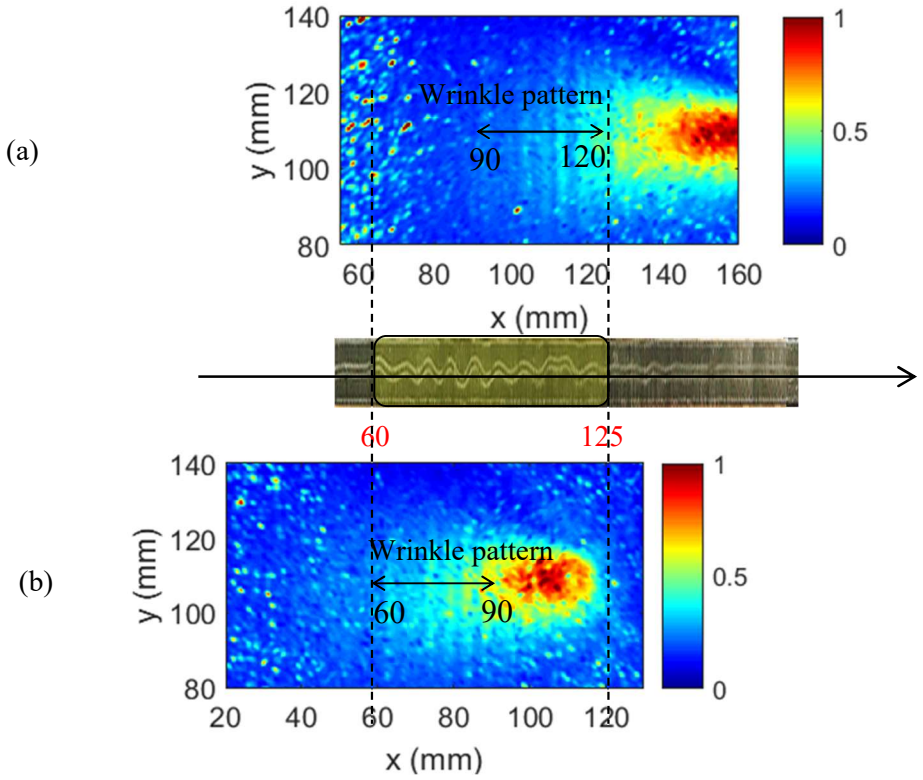


Figure 11.24: Energy map imaging of wrinkle region generated with (a) ACT actuation at x = 160 mm, (b) ACT actuation at x = 110 mm (Courtesy of NASA Langley Research Center and Boeing)

To imaging the wrinkle on the left side of the 90 mm location, the ACT transducer is then moved to the left to 110 mm location and the imaging result is given in Figure

11.24b. The wrinkle imaging in the 60 mm to 90 mm is noted. Therefore, from Figure 11.24a and b, the entire wrinkle region from 60-125 mm is successfully imagined.

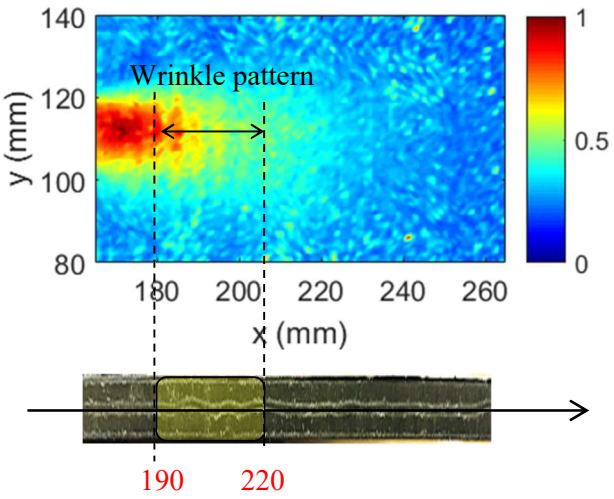


Figure 11.25: Energy map imaging of the reference region (Courtesy of NASA Langley Research Center and Boeing)

In the reference region imaging (Figure 11.25), some wrinkle pattern around 180 to 200 mm is noted, which is consistent with the R3 linescan inspection result and confirms that subtle wrinkle damage is also existing in the reference region.

11.2.3 WRINKLE INSPECTION ALONG THE *Y*-AXIS DIRECTION

In this section, the wrinkle inspection along the *y*-axis direction is performed. Three linescans R1, R2, and R3 in the reference regions and three linescans W1, W2, and W3 in the wrinkle region as illustrated in Figure 11.26a are conducted to collect the wavefields from the wrinkle and the reference areas for comparative analysis.

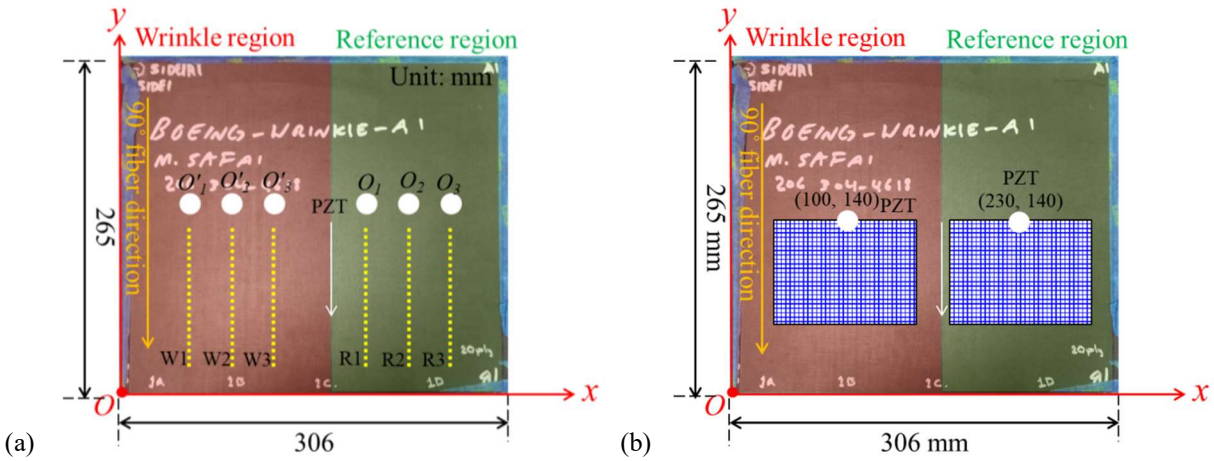


Figure 11.26: Experimental setup for specimen A1 along 90°/270° w.r.t actuation on side 1: (a) line inspection, and (b) area inspection (Courtesy of NASA Langley Research Center and Boeing)

First, the collected wavefields of R1, R2, and R3 from the reference region are given in Figure 11.27a, b, and c. From all these wavefields, no reflections are observed in these wavefields. The frequency wavenumber spectrums are then obtained and plotted in Figure 11.27d, e, and f, respectively. It is noted that no negative wavenumbers observed in the wavenumber spectra as well, demonstrating that in the reference region, through linescan along the y-axis direction, wrinkle signature is not captured.

Next, the linescan wavefields collected from the wrinkle region are presented in Figure 11.28a, b, and c for W1, W2, and W3. No reflections are noted in all the three wavefields. Moreover, no negative wavenumbers which represent the reflections are seen from the frequency wavenumber spectra in Figure 11.28d, e, and f. The result shows that it is challenging to conduct linescan inspection of the wrinkle along the *y*-axis direction.

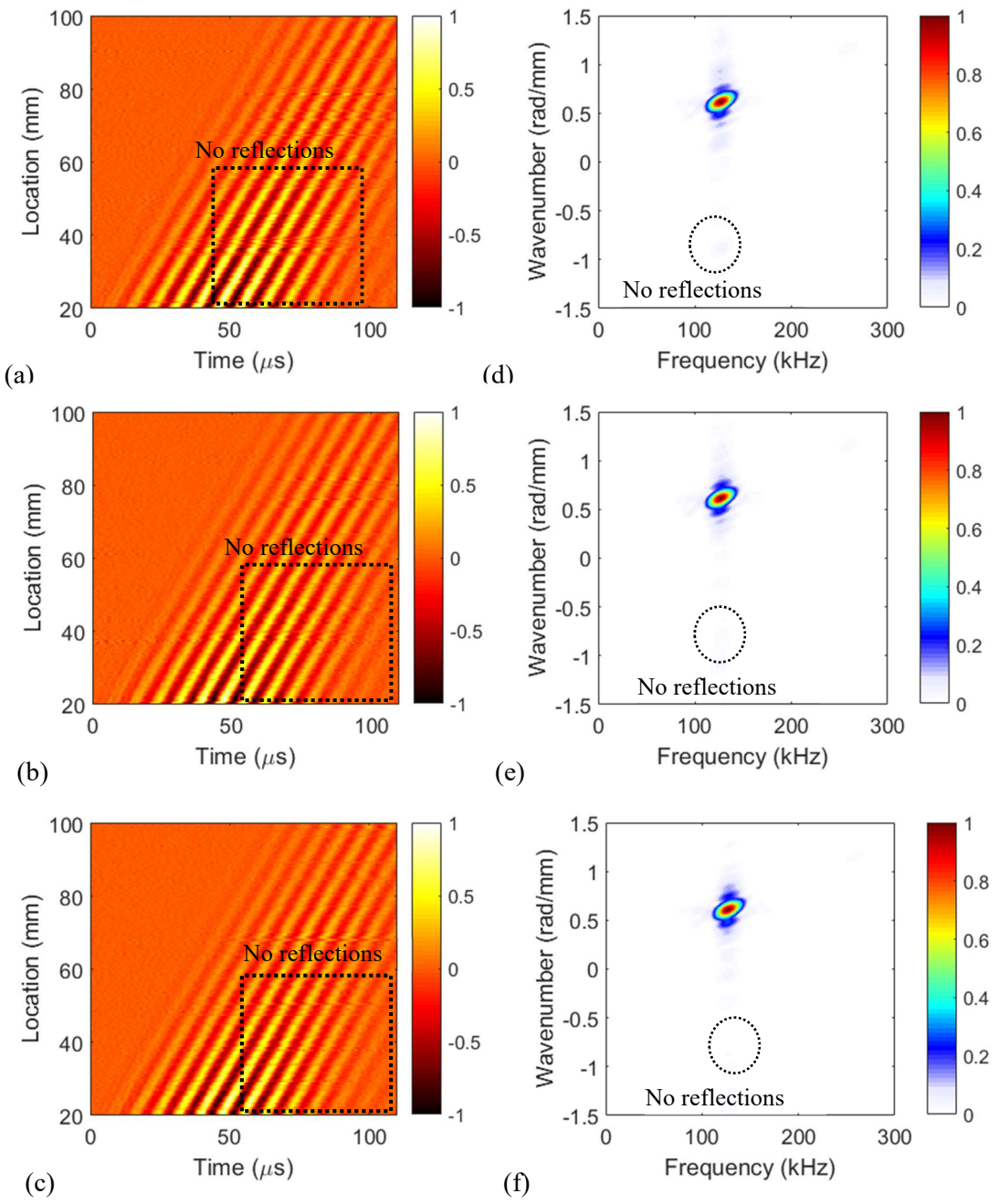


Figure 11.27 : 1D time-space wavefields of R1, R2, and R3 in (a), (b), and (c) respectively and their frequency-wavenumber spectra in (d), (e), and (f), respectively

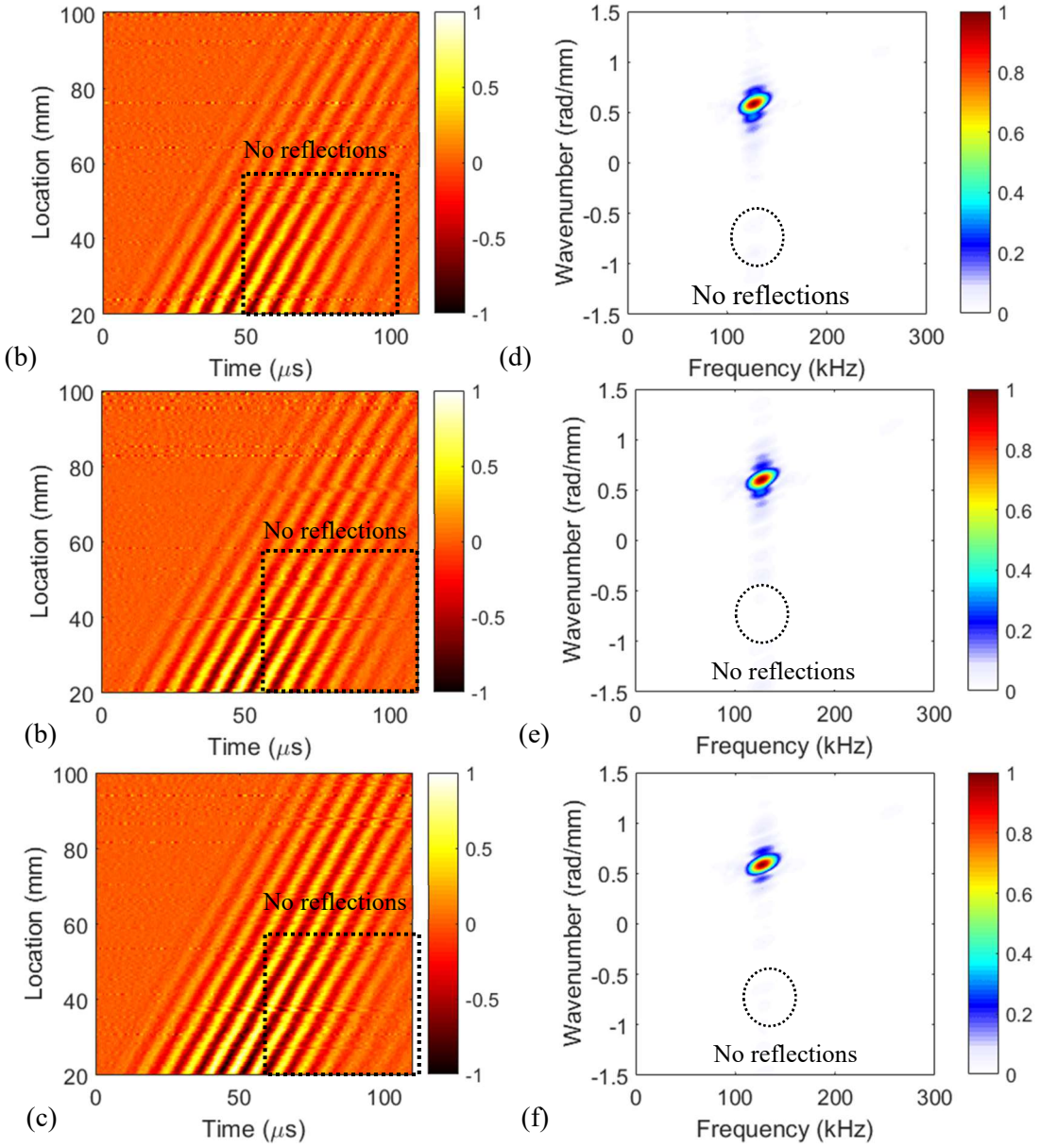


Figure 11.28: 1D time-space wavefields of W1, W2, and W3 in (a), (b), and (c) respectively and their frequency-wavenumber spectra in (d), (e), and (f), respectively

2D area inspection along *y*-axis direction was then conducted. The 2D scan in the reference region and the wrinkle region is illustrated in Figure 11.26b. The obtained wavefields at 25 μs and 50 μs for the wrinkle region were given in Figure 41a, and the wavefields of reference region at 25 μs and 50 μs are shown in Figure 41b. By comparing

the wavefields at 25 μs of the reference region and wrinkle region, no significant difference was observed. However, for the wavefields at 50 μs, it is seen that the stronger wave strength is observed in the left side in the wrinkle region, while more evenly distributed wave strength is observed in the reference region.

Then the energy map method was applied, and the obtained energy maps were plotted in Figure 11.30a and b for wrinkle region and reference region. The energy image of the reference region shows the energy attenuated along the propagating path. For the energy map of the wrinkle region, it shows except for the attenuation phenomenon, there is an energy concentrated band in the energy map, but we cannot relate it to the wrinkle in the plate. No wrinkle related signature can be observed in the area inspection result.

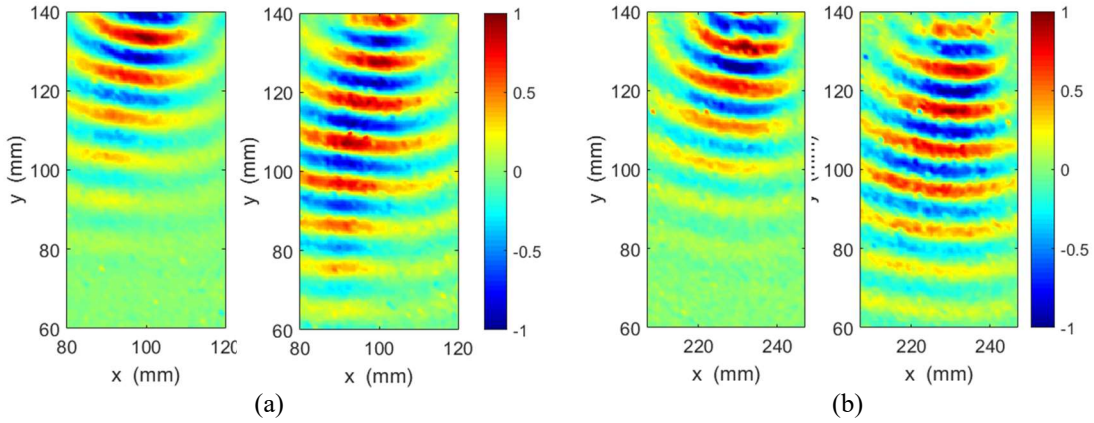


Figure 11.29: Wavefields at 50 μs: (a) wrinkle region, and (b) reference region

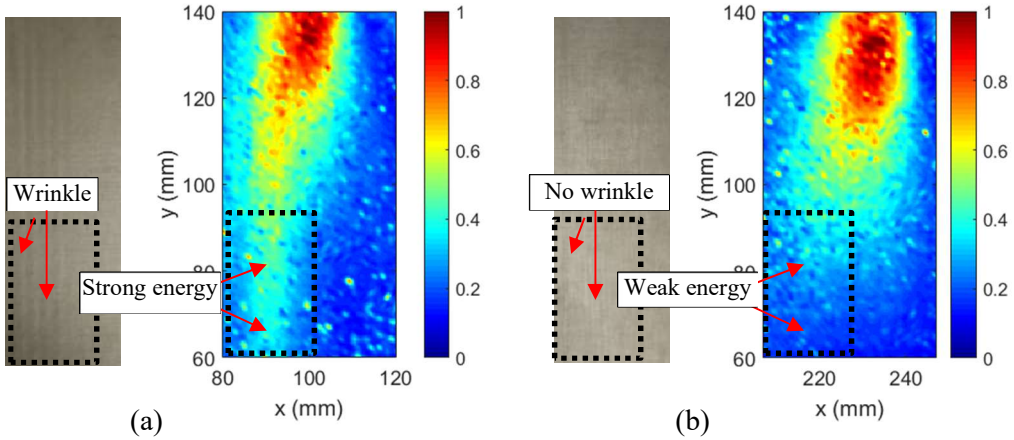


Figure 11.30: Energy map imaging: (a) wrinkle region, and (b) reference region (Courtesy of NASA Langley Research Center and Boeing)

Overall, with the ACT-SLDV Lamb wave methods, wrinkle defects in a selected specimen can (or cannot?) be observed through strong modifications in the wavefield, wave energy distribution map, as well as the frequency-wavenumber spectra. It proves to be an effective means for such defect inspection in laminated composite with the presented results.